

Impact of Spectral Transition Zone in Reference ENIGMA Configuration

G. Aliberti, G. Palmiotti, and T. A. Taiwo

Nuclear Engineering Division
Argonne National Laboratory
9700 South Cass Avenue
Argonne, IL 60439

J. Tommasi

CEA-CADARACHE
DER/SPRC/LEPh - Bât.230
13108 St.-Paul-Lez-Durance (FRANCE)

August 31, 2005

Table of Contents

I. Introduction.....	5
II. Core Configurations for Study	7
III. Calculation Models and Tools.....	9
IV. Impact of Transition Zone on Neutron Flux Distributions.....	12
V. Impact on Core Reactivity.....	14
VI. Spectral Index Variations.....	21
VII. Conclusions.....	24
References	26

List of Figures

Figure 1. ENIGMA Reference Fuel Assembly.	7
Figure 2. ENIGMA Radial (XY-Plane) Core Layout.	8
Figure 3. ENIGMA RZ Geometry.	9
Figure 4. Direct Flux Spectrum - PIT Heterogeneous.	12
Figure 5. Adjoint Flux Spectrum – PIT Heterogeneous.	12

List of Tables

Table 1. Region Homogenized Compositions [10^{24} at/cm ³].	10
Table 2. Spectrum Hardness Parameter, r.	12
Table 3. BISTRO Reactivity Results (pcm).	14
Table 4. TGV/VARIANT Reactivity Results (pcm).	14
Table 5. Exact Perturbation Components [pcm] for $\Delta\rho = \rho_{\text{void_transition}} - \rho_{\text{reference}}$ (Heterog.).	15
Table 6. Exact Perturbation Components [pcm] for $\Delta\rho = \rho_{\text{graphite_transition}} - \rho_{\text{reference}}$ (Heterog.).	16
Table 7. Exact Perturbation Components by Neutron Energy Group (Heterogeneous) [pcm].	16
Table 8. Exact Perturbation Components [pcm] for $\Delta\rho_{\text{reference}} = \rho_{\text{homogeneous_pit}} - \rho_{\text{heterogeneous_pit}}$.	17
Table 9. Exact Perturbation Components [pcm] for $\Delta\rho_{\text{void_transition}} = \rho_{\text{homogeneous_pit}} - \rho_{\text{heterogeneous_pit}}$.	18
Table 10. Exact Perturbation Components [pcm] for $\Delta\rho_{\text{graphite_transition}} = \rho_{\text{homogeneous_pit}} - \rho_{\text{heterogeneous_pit}}$.	18
Table 11. Exact Perturbation Components by Energy Group for the Reference Config. [pcm].	18
Table 12. Sensitivity Coefficients by Isotopes [pcm] for $\Delta\rho = \rho_{\text{void_transition}} - \rho_{\text{reference}}$ (Heterog.).	19
Table 13. Sensitivity Coefficients by Isotopes [pcm] for $\Delta\rho = \rho_{\text{graphite_transition}} - \rho_{\text{reference}}$ (Heterog.).	20
Table 14. Sensitivity Coefficients by Group [pcm] for $\Delta\rho = \rho_{\text{void_transition}} - \rho_{\text{reference}}$ (Heterog.).	20
Table 15. Sensitivity Coefficients [pcm] for $\Delta\rho = \rho_{\text{graphite_transition}} - \rho_{\text{reference}}$ (Heterogeneous).	20
Table 16. Spectral Indices for ENIGMA Configurations.	21
Table 17. Exact Perturbation Components for $\frac{\langle \sigma_{\text{U8}} \Phi \rangle}{\langle \sigma_{\text{U5}} \Phi \rangle} \Big _{(\text{Void Transition} - \text{Ref.})/\text{Ref.}}$ (Heterogeneous).	22
Table 18. Exact Perturbation Components for $\frac{\langle \sigma_{\text{Pu9}} \Phi \rangle}{\langle \sigma_{\text{U5}} \Phi \rangle} \Big _{(\text{Void Transition} - \text{Ref.})/\text{Ref.}}$ (Heterogeneous).	22
Table 19. Exact Perturbation Components for $\frac{\langle \sigma_{\text{U8}} \Phi \rangle}{\langle \sigma_{\text{U5}} \Phi \rangle} \Big _{(\text{Graphite Transition} - \text{Ref.})/\text{Ref.}}$ (Heterogeneous).	22
Table 20. Exact Perturbation Components for $\frac{\langle \sigma_{\text{Pu9}} \Phi \rangle}{\langle \sigma_{\text{U5}} \Phi \rangle} \Big _{(\text{Graphite Transition} - \text{Ref.})/\text{Ref.}}$ (Heterogeneous).	22
Table 21. Exact Perturbation Components by Energy Group.	23

I. Introduction

The gas-cooled fast reactor (GFR) is one of six advanced nuclear energy systems being studied under the auspices of the Gen IV International Forum (GIF). In a bilateral International Nuclear Energy Research Initiative (I-NERI) project French and U.S. national laboratories, industry, and universities are collaborating on the development of the GFR. This effort is led by the ANL in the U.S. and the CEA in France.

Some of the attractions of the GFR include:

- Hard spectrum and core breeding ratio, $BR \approx 1$. These features allow minimal waste production, improved transmutation capability, optimal and flexible use of natural resources, potentially better economy (because of use of higher power density relative to current thermal gas-cooled systems), and improved non-proliferation (no fertile blanket);
- Temperature resistant fuel and structure elements that are favorable to tight fission product confinement and system operation at high temperature;
- High temperature and transparent helium (He) gas coolant that allows a high thermodynamic conversion efficiency, other energy applications (e.g., hydrogen production), and ease of in-service inspection and repair;
- Possible direct energy conversion cycle leading to a simpler design, increased conversion efficiency, and lower investment costs.

The French strategy for advanced systems includes the development of the GFR and sodium-cooled fast reactor (SFR) to levels that allow industries to be able to make an informed choice of the fast spectrum system that would provide a sustainable nuclear energy generation option for the future. Current planning calls for the construction of a small experimental research and technology development reactor (ETDR) around 2009 (first operation in 2015) at CEA-Cadarache, France. This would be followed by the construction of a GFR industrial prototype, around 2025. In support of the GFR development efforts, a new physics experimental program (called ENIGMA, Experimental Neutron Investigation of Gas-cooled reactor at MASURCA) is being planned for Cadarache. This new experiment would provide better understanding of GFR neutronic features and will be the basis for the extension of current neutronics code validation domain (particularly, the ERANOS code system in France) to the analysis of GFRs.

Experimental planning and decisions are ongoing for ENIGMA. One of the items that have been evaluated is the feasibility of obtaining different flux spectra in the ENIGMA reference configuration, giving the flexibility of simulating a large series of proposed gas-cooled fast systems with harder or softer spectra. In order to achieve this goal it was proposed to use a spectral transition zone in the center region of the ENIGMA core configuration. Another goal of the study is to evaluate the impact of the graphite cross-sections on the performance characteristics of the MASURCA configurations.

The work was supported by ANL, through the residence of one of the authors at CEA-Cadarache in 2005. In this report, the impacts of the transition zone on the core physics parameters of the reference ENIGMA configuration are summarized.

II. Core Configurations for Study

The reference configuration for the ENIGMA first core has been developed [1]. The core is uniformly loaded with 85 fuel subassemblies (PIT assemblies) each containing 24 $UPuO_2$, 8 UO_2 , 16 graphite (C) and 16 void rodlets (see Figure 1). Graphite is used in the subassembly to imitate carbide fuel and to represent matrix and structural elements; there is no plan to manufacture new fuel forms in early phases of the ENIGMA project, so existing materials are used in representative proportions. The fueled zone is surrounded radially and axially by a reflector zone and an outer shield zone (stainless steel).

For the purpose of this study, it is assumed that the transition zone would be in the core interior and comprises the central six subassemblies (4 full and 4 half subassemblies) shown in Figure 2. To obtain spectral transition zones, two different modifications to these assemblies have been considered. In these cases, the central zone would contain either of the following:

- Subassemblies in which the 16 void rodlets are replaced by 16 graphite rodlets (i.e., PIT assemblies with 32 graphite rodlets). This provides a softer spectrum because of the increased graphite content. This is called the graphite transition zone configuration.
- Alternatively, subassemblies in which the 16 graphite rodlets are replaced by 16 void rodlets (i.e., PIT assemblies with 32 void rodlets), to provide a harder spectrum.

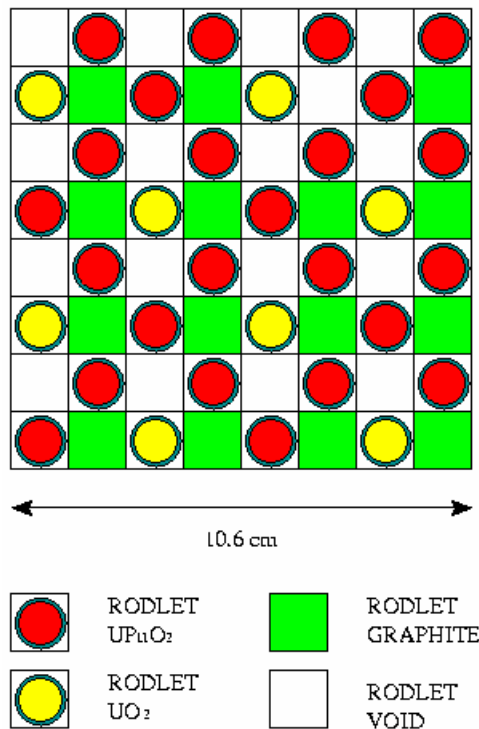


Figure 1. ENIGMA Reference Fuel Assembly.

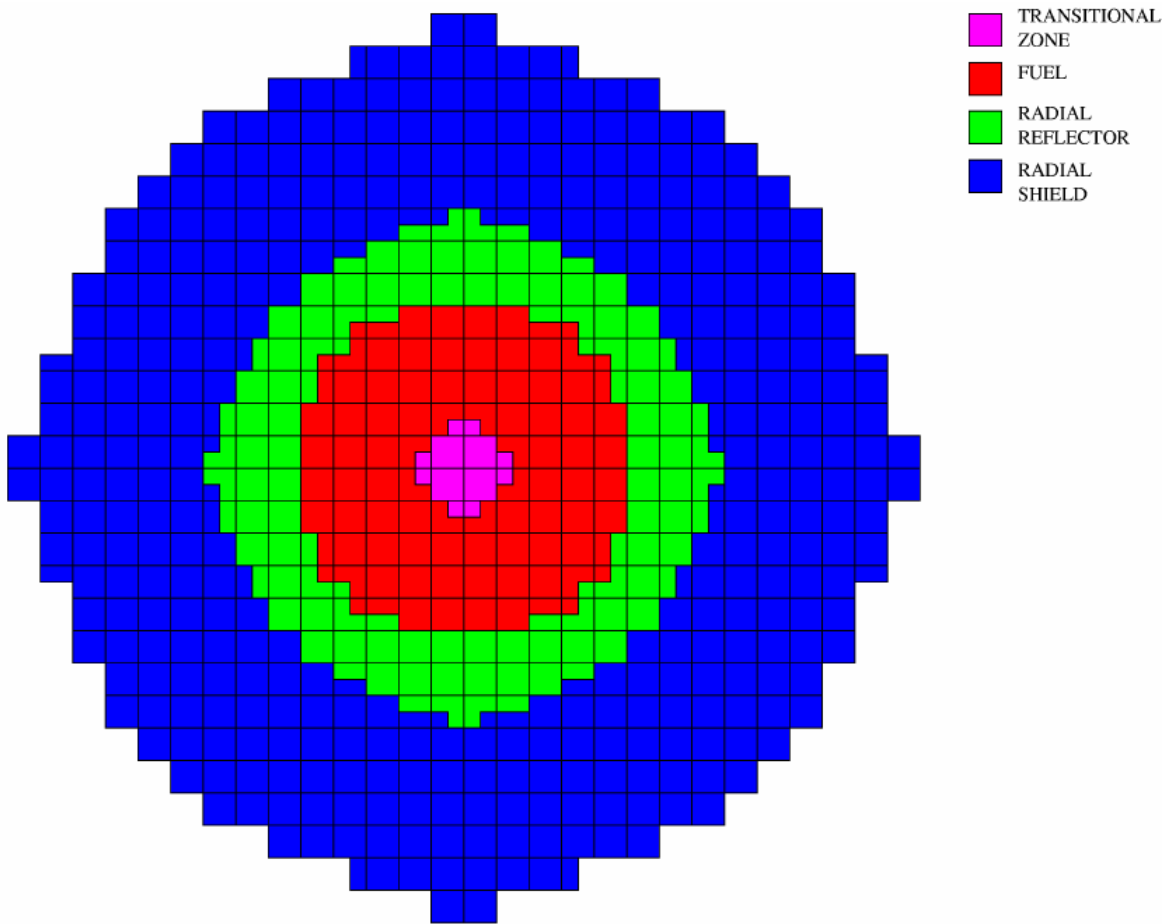


Figure 2. ENIGMA Radial (XY-Plane) Core Layout.

III. Calculation Models and Tools

In the present study, the introduction of the transition zone is investigated through its effects on the neutron flux distributions, reactivity and spectral indices variations. These parameters were calculated using the European ERANOS code system [2]. Neutron cross-sections for the calculations have been processed into a 33 multigroup energy structure using the ECCO code [3] with the ERALIB1 data library [4]. Neutron fluxes were calculated using the BISTRO code [5] in RZ geometry and the S_4P_1 approximation. This code option was selected because it has a robust and well-tested perturbation capability for investigating the reasons for differences between two core configurations/calculations. Previous analyses of fast reactor experiments have demonstrated the accuracy of the RZ model for reactivity, spectral indices and flux calculations for the MASURCA core, particularly if there is no core asymmetry and local flux details are not required.

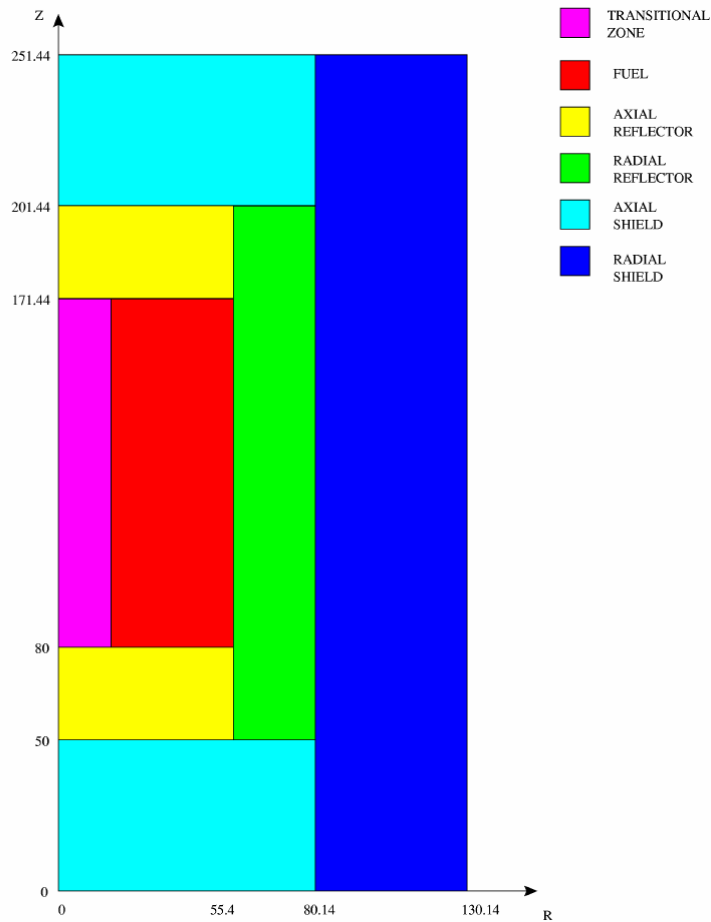


Figure 3. ENIGMA RZ Geometry.

The RZ model of the reference ENIGMA core that has been developed is shown in Fig. 3. For the analysis of such fast reactor models, region homogenized nuclide densities are employed for the generation of the multigroup neutron cross-sections. This approach is called the homogeneous

model. The homogenized compositions (nuclide densities) are provided in Table 1 for the base assembly (PIT), the modified assemblies (PIT with 32 void or graphite rodlets), and the axial and radial reflectors and shields.

Table 1. Region Homogenized Compositions [10^{24} at/cm³].

	PIT	PIT with 32 Void Rodlets	PIT with 32 Graphite Rodlets	Axial Reflector	Radial Reflector	Axial Shield	Radial Shield
U234	6.26220E-07	6.26220E-07	6.26220E-07				
U235	2.75384E-05	2.75384E-05	2.75384E-05				
U236	1.27430E-06	1.27430E-06	1.27430E-06				
U238	5.79480E-03	5.79480E-03	5.79480E-03				
Np237	1.65462E-06	1.65462E-06	1.65462E-06				
Pu238	2.08333E-06	2.08333E-06	2.08333E-06				
Pu239	1.14127E-03	1.14127E-03	1.14127E-03				
Pu240	2.76140E-04	2.76140E-04	2.76140E-04				
Pu241	1.28586E-05	1.28586E-05	1.28586E-05				
Pu242	9.95066E-06	9.95066E-06	9.95066E-06				
Am241	5.05871E-05	5.05871E-05	5.05871E-05				
Fe54	3.54712E-04	4.14976E-04	2.94447E-04	2.61766E-03	2.61766E-03	3.23041E-03	4.57985E-03
Fe56	5.56821E-03	6.51423E-03	4.62219E-03	4.10917E-02	4.10917E-02	5.10739E-02	7.24090E-02
Fe57	1.28595E-04	1.50442E-04	1.06747E-04	9.48984E-04	9.48984E-04	1.22533E-03	1.73718E-03
Fe58	1.71135E-05	2.00211E-05	1.42060E-05	1.26292E-04	1.26292E-04	1.67090E-04	2.36889E-04
Cr50	7.21863E-05	8.42837E-05	6.00888E-05	5.25611E-04	5.25611E-04	6.52073E-04	3.88182E-05
Cr52	1.39204E-03	1.62533E-03	1.15876E-03	1.01359E-02	1.01359E-02	1.25603E-02	7.47719E-04
Cr53	1.57846E-04	1.84299E-04	1.31393E-04	1.14933E-03	1.14933E-03	1.42407E-03	8.47754E-05
Cr54	3.92913E-05	4.58759E-05	3.27066E-05	2.86092E-04	2.86092E-04	3.53768E-04	2.10600E-05
Ni58	5.47945E-04	6.48677E-04	4.47214E-04	4.31294E-03	4.31294E-03	5.01450E-03	7.44874E-04
Ni60	2.11068E-04	2.49869E-04	1.72266E-04	1.66134E-03	1.66134E-03	1.91707E-03	2.84770E-04
Ni61	9.17496E-06	1.08616E-05	7.48827E-06	7.22172E-05	7.22172E-05	8.29996E-05	1.23291E-05
Ni62	2.92538E-05	3.46316E-05	2.38759E-05	2.30260E-04	2.30260E-04	2.63689E-04	3.91694E-05
Ni64	7.45007E-06	8.81965E-06	6.08048E-06	5.86404E-05	5.86404E-05	6.68404E-05	9.92875E-06
O	1.45532E-02	1.45532E-02	1.45532E-02				
C	1.96036E-02	2.71415E-05	3.91801E-02	1.21638E-04	1.21638E-04	5.19968E-06	2.90417E-03
Al	6.01452E-07	6.01452E-07	6.01452E-07				
Mn	1.00717E-04	1.22551E-04	7.88822E-05	9.13875E-04	9.13875E-04		
Mo	1.59449E-05	1.62209E-05	1.56690E-05	2.66176E-05	2.66176E-05	3.49181E-06	3.49181E-06
Si	8.22729E-05	9.93568E-05	6.51889E-05	7.16529E-04	7.16529E-04	2.81155E-05	2.81155E-05
Ti	6.90972E-07	7.51446E-07	6.30497E-07	2.97681E-06	2.97681E-06	4.99779E-07	4.99779E-07
Cu	1.95177E-06	2.73295E-06	1.17058E-06	3.14028E-05	3.14028E-05	7.71376E-05	7.05761E-04
B10	1.40240E-12	1.40240E-12	1.40240E-12			1.00000E-15	1.00000E-15
Zr	8.17728E-12	8.17728E-12	8.17728E-12	6.25169E-12	6.25169E-12		
V				1.84606E-05	1.84606E-05		
Co59				7.15335E-05	7.15335E-05		
H						1.63827E-06	1.63827E-06
Nb93						7.72677E-07	7.72677E-07

Because of the utilization of graphite in the core to represent carbide fuel and matrix and structural materials, and the use of voided rodlets to account for neutron streaming from potential GFR designs, it is quite possible that the simple homogenization of the fuel zone might introduce additional errors. As a result, an additional approach for generating the multigroup cross-sections has been investigated in this work. In this approach the heterogeneous model of the subassembly is used in the ECCO code for the generation of homogenized subassembly cross-sections. This is called the heterogeneous model.

Finally, for sensitivity study of the solution approach, calculations using the TGV/VARIANT (variational nodal transport) code [6] in XYZ geometry have been performed. In these calculations, the anisotropic scattering order 1 and the full P_3 angular flux approximations are utilized.

IV. Impact of Transition Zone on Neutron Flux Distributions

As aforementioned, one primary reason for introducing a transition zone is to create configurations characterized by different neutron spectra. The impact of the transition zone on the direct and adjoint flux distributions have been calculated using the BISTRO code. Figures 4 and 5 display the direct and adjoint flux spectra at the core center (R=0; Z=125.72cm) of each configuration: the reference case refers to the reference configuration without a transitional zone; while the label “Void” or “Graphite (C) Transition Zone” corresponds to the calculation using a transition zone consisting of PIT assemblies with 32 void or 32 graphite rodlets (see Section II for details). Results for both the homogeneous and heterogeneous models are presented.

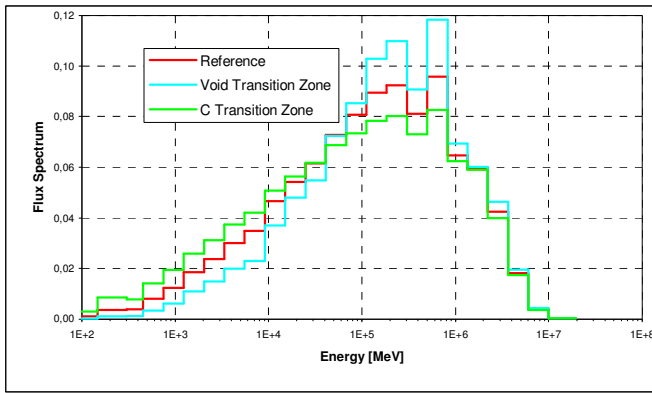


Figure 4. Direct Flux Spectrum - PIT Heterogeneous.

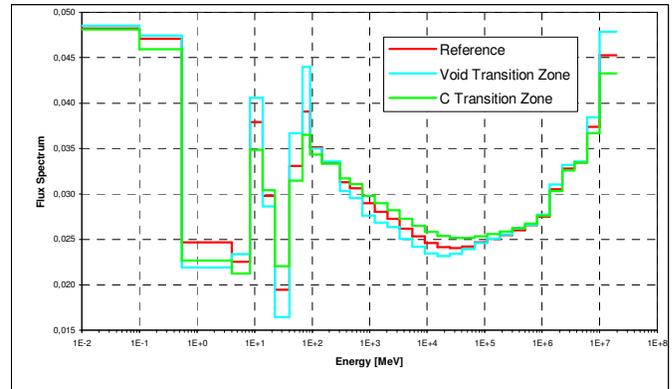


Figure 5. Adjoint Flux Spectrum – PIT Heterogeneous.

For this study, the fluxes have been normalized by setting to unity, the sum over the energy groups. The spectrum hardness parameter ($r = v\Sigma_f/\xi\Sigma_s$), given in Table 2 for each configuration, can also be used to characterize the neutron spectrum. When comparing two configurations, a higher value of r denotes a harder spectrum.

Table 2. Spectrum Hardness Parameter, r .

Reference	Void Transition Zone	Graphite Transition Zone
.317	.500	.249

As expected, it is observed that the use of a graphite transition zone has the effect of producing a softer spectrum compared to the reference case. The void transition zone on the other hand produces a harder spectrum. These spectra shifts are also captured by the hardness parameter, r . With the void transition zone, the value of the parameter is ~60% higher than for the reference configuration. That for the graphite transition zone is about 20% less. However, note that the values shown in Table 2

have been obtained from the cell calculation for the transition zone in fundamental mode; since this zone in the real configuration is associated to a finite volume, those values are indicative of the parameter r that most likely would be attained asymptotically at the center of the zone.

These results indicate that it is possible to effect large spectral variations by the use of the central transition zones. Such latitude permits the tailoring of the ENIGMA configuration to represent the spectra of potential GFR designs, even those for which the exact core materials might not be available for ENIGMA tests.

V. Impact on Core Reactivity

The “reactivity” for each core configuration has been calculated using the expression $(1-1/k_{\text{eff}}) \times 10^5$ (pcm), where k_{eff} is the core multiplication factor. The reactivity results for all the cases are presented in Tables 3 and 4 (results from BISTRO and TGV/VARIANT calculations, respectively). It is noted that the convergence criteria for the k_{eff} is 1.E-5 in the BISTRO calculations and 5.E-6 in the VARIANT calculations. Besides the core reactivity, the difference between the values for configurations with a transition zone and that of the reference configuration is also provided (in brackets). Additionally, the tables contain the impact of the heterogeneity effect on the core reactivity calculation (difference between the heterogeneous and homogeneous values). This effect is included because they were unexpectedly found more important than in sodium-cooled MASURCA cells (for instance, the MUSE-4 configurations).

Table 3. BISTRO Reactivity Results (pcm).

	Reference	Void Transition Zone	Graphite Transition Zone
Pit Heterogeneous	385	412 (+27)	477 (+92)
Pit Homogeneous	-58	45 (+103)	-61 (-3)
Heterogeneous Effect	-443	-367	-537

Table 4. TGV/VARIANT Reactivity Results (pcm).

	Reference	Void Transition Zone	Graphite Transition Zone
Pit Heterogeneous	178	193 (+15)	273 (+95)
Pit Homogeneous	-261	-169 (+92)	-261 (0)
Heterogeneous Effect	-439	-362	-534

Heterogeneity Effect

The impact of the heterogeneity effect is not negligible for these core configurations contrary to previous observations for most MASURCA test configurations; this effect has however been previously found to be significant for some core configurations, particularly for plate geometries. For the ENIGMA configurations, the heterogeneity effect could be as large as ~500 pcm. The larger heterogeneity effect, compared to standard sodium-cooled type configuration, is to be attributed to the presence of the void rodlets in the reference cell: smearing the void leads to a larger heterogeneity effect. It is noted that this effect is evident in all configurations. In fact, the results show that the effect is highest for the configuration with the graphite transition zone, and lowest for the configuration with the void transition zone. This trend indicates the effect is more pronounced as the neutron spectrum becomes softer, as would be expected intuitively, because of the self-shielding in the resonance region and because of the mean neutron lifetime increase.

Reactivity Values

Tables 3 and 4 show that the BISTRO and TGV/VARIANT codes predict very similar core reactivity for each of the three configurations (reference, void and graphite transition zone). The maximum difference is about 200 pcm, with the BISTRO calculation giving the higher value. This difference is likely due to the use of the approximate RZ geometry in the BISTRO calculation and the difference of using S_4 discrete ordinates in one approach (BISTRO) and P_3 angular flux approximation in the other. It is observed that the BISTRO and TGV/VARIANT codes provide consistent results for the reactivity variation due to the introduction of the transition zones as well as for the heterogeneity effects.

Of particular interest in the reactivity results is the fact that the introduction of either the void or graphite transition zones gives a higher k_{eff} (reactivity) than the reference case. While these differences are small, an attempt has been made to provide explanations for them using perturbation theory (see next subsection). The resolution of this difference is also one major reason why the TGV/VARIANT solution approach was used in this study.

Perturbation Theory Analysis of Differences

An evaluation of the reactivity differences between the reference configuration and the configurations with the void and graphite transition zones has been performed, using perturbation theory. The results for these cases are summarized in Tables 5 to 7. These results were obtained using the exact perturbation theory option with BISTRO; the exact perturbation theory option is used because it was observed that effects of interest are non-linear (otherwise, the total effect shown in the last row of Tables 5 and 6 would be -42.5 and +51.7 pcm, respectively, for a first-order perturbation calculation).

Table 5. Exact Perturbation Components [pcm] for $\Delta\rho = \rho_{\text{void_transition}} - \rho_{\text{reference}}$ (Heterogeneous).

Isotope	Capture	Fission	Leakage	Elastic	Inelastic	N,xN	Total
U238	31.7	-8.6	-3.8	-1.7	3.2	0.1	20.9
Pu239	4.1	-36.9	-0.6	-0.3	0.5	0.0	-33.1
Pu240	1.0	-4.4	-0.2	-0.1	0.1	0.0	-3.6
Fe56	-8.7	0.0	7.5	-5.0	-24.5	0.0	-30.7
Cr52	-1.7	0.0	2.8	-1.9	-5.2	0.0	-6.0
Ni58	-5.7	0.0	1.6	-1.4	-2.0	0.0	-7.5
O	0.5	0.0	-4.9	-12.6	0.0	0.0	-17.0
C	8.4	0.0	-248.2	340.1	12.9	0.0	113.3
Other	-9.5	-1.3	3.7	-1.1	-5.0	0.1	-13.2
Total	20.1	-51.2	-242.1	316.0	-20.0	0.2	23.1

Table 6. Exact Perturbation Components [pcm] for $\Delta\rho = \rho_{\text{graphite_transition}} - \rho_{\text{reference}}$ (Heterogeneous).

Isotope	Capture	Fission	Leakage	Elastic	Inelastic	N,xN	Total
U238	-60.5	6.3	3.5	0.9	-2.8	-0.1	-52.6
Pu239	-14.1	46.9	0.7	0.2	-0.5	0.0	33.1
Fe56	11.6	0.0	-8.7	0.6	23.7	0.0	27.2
Cr52	2.5	0.0	-2.2	1.3	5.1	0.0	6.6
Ni58	5.8	0.0	-1.8	-0.9	2.0	0.0	5.1
O	-0.4	0.0	3.3	7.0	0.0	0.0	9.9
C	-7.4	0.0	193.3	-120.9	-12.1	0.0	52.8
Other	10.7	5	-4.4	-3.2	4.6	0	12.9
Total	-51.8	58.2	183.7	-115.0	20.0	-0.1	95.0

Table 7. Exact Perturbation Components by Neutron Energy Group (Heterogeneous) [pcm].

Gr.	Energy [eV]	$\Delta\rho = \rho_{\text{void_transition}} - \rho_{\text{reference}}$				$\Delta\rho = \rho_{\text{graphite_transition}} - \rho_{\text{reference}}$			
		U238 Capture	Pu239 Fission	C Leakage	C Elastic	U238 Capture	Pu239 Fission	C Leakage	C Elastic
1	1.9640E+7	0.0	-0.7	-3.3	6.1	0.0	0.7	2.4	-5.6
2	6.0653E+6	0.2	-6.5	-45.0	80.6	-0.1	6.5	31.6	-76.3
3	2.2313E+6	-0.1	-2.4	-28.0	119.6	0.0	3.0	23.5	-120.2
4	1.3534E+6	1.1	-11.4	-66.9	129.8	-0.6	7.6	36.4	-108.2
5	4.9787E+5	0.6	-3.8	-46.9	113.9	-0.4	3.2	25.7	-93.4
6	1.8316E+5	0.9	-0.1	-37.8	93.3	-0.5	0.7	23.6	-81.4
7	6.7379E+4	2.5	2.7	-17.3	10.9	-1.6	-0.6	18.0	-9.6
8	2.4788E+4	4.8	0.7	-8.0	-80.3	-4.2	0.0	13.7	101.8
9	9.1188E+3	6.9	0.9	-1.6	-84.6	-12.1	1.6	11.5	144.1
10	2.0347E+3	12.5	-18.3	3.2	-39.9	-27.6	18.9	6.4	93.3
11	4.5400E+2	2.1	1.5	3.0	-9.4	-13.6	5.0	1.0	34.7
12	2.2603E+1	0.2	-0.3	0.4	0.2	0.3	0.5	-0.4	0.0
13	4.0000E+0	0.0	0.9	0.1	0.0	0.0	-0.2	-0.1	0.0
14	5.4000E-1	0.0	0.0	0.0	0.0	0.0	0.0	0.0	0.0
15	1.0000E-1	0.0	0.0	0.0	0.0	0.0	0.0	0.0	0.0
Total		31.7	-36.9	-248.2	340.1	-60.5	46.9	193.3	-120.9

Tables 5 and 6 show the exact perturbation components (by isotopes) of the reactivity differences between the reference configuration and the configurations with the void and graphite transition zones, respectively. The breakdowns by neutron energy group for these differences are provided in Table 7.

It is observed that the reactivity variations between the reference and the transition-zone cases arise mainly from a compensation of effects between the transport (leakage) and the elastic components of graphite (C). However, the signs of these components are different for the two comparisons (i.e., “void transition zone – reference” and “graphite transition zone – reference”). Specifically, for the comparison of the void transition zone and reference configurations, the harder spectrum of the void transition zone increases the neutron leakage, while the graphite slows the neutrons down to lower energy by elastic scattering, giving an overall positive change in the k_{eff} , which dominates the negative effect coming from the leakage. These components are reversed when comparing the

configuration with the graphite transition zone to the reference one. However, in both cases, the component with the positive sign dominates.

Other minor contributions are due to the U-238 capture and Pu-239 fission reactions. Those contributions are mainly in the energy range of the unresolved resonances (see Table 7).

The main reasons for the differences between the “heterogeneous” to “homogeneous” results have also been evaluated using perturbation theory. Results are summarized in Tables 8, 9, and 10, for the reference, void transition zone, and graphite transition zone configurations, respectively. The breakdown of the differences by energy group is presented in Table 11 for the reference case.

For all the cases, the difference can be attributed to the misprediction of the resonance self-shielding cross-sections of U-238 capture and Pu-239 capture and fission. The transport (leakage) and elastic contributions of graphite (C) are secondary, but also significant. Additionally, some non-negligible contributions are due to the oxygen (O) leakage components. It is noted that the higher values of the heterogeneity effects observed for the gas-cooled compared to the Na-cooled MASURCA cells are due to the increased leakage component in the streaming channels, which is practically minimized when using a homogenized cell. The breakdown by energy group shows that the significant leakage components, as expected, are mainly located in the energy range where the flux spectrum is more important, while the capture and fission components of the fissile isotopes are located in the unresolved resonance energy range, because of the self-shielding effects. The elastic reaction of graphite gives contributions in both energy ranges.

Table 8. Exact Perturbation Components [pcm] for $\Delta\rho_{\text{reference}} = \rho_{\text{homogeneous_pit}} - \rho_{\text{heterogeneous_pit}}$.

Isotope	Capture	Fission	Leakage	Elastic	Inelastic	N,xN	Total
U238	-549.4	-71.4	102.0	2.0	36.7	-1.6	-481.6
Pu239	-387.0	380.6	16.8	0.5	15.8	-0.3	26.3
Pu240	-94.2	-74.0	4.3	0.2	4.0	-0.1	-159.8
Am241	-20.7	-17.6	0.5	0.0	0.7	0.0	-37.1
Fe56	-48.0	0.0	8.6	-4.2	-15.4	0.0	-58.9
Cr52	-6.3	0.0	-2.0	-0.2	-3.8	0.0	-12.3
Ni58	-2.8	0.0	-2.0	2.4	-1.1	0.0	-3.5
O	6.7	0.0	96.6	24.1	1.3	0.0	128.7
C	-2.3	0.0	277.7	-110.0	-2.9	0.0	162.4
Other	12.3	5.7	2.1	0.1	-2.6	0.0	-7.0
Total	-1116.3	223.3	504.6	-85.1	32.7	-2.0	-442.8

Table 9. Exact Perturbation Components [pcm] for $\Delta\rho_{\text{void_transition}} = \rho_{\text{homogeneous_pit}} - \rho_{\text{heterogeneous_pit}}$

Isotope	Capture	Fission	Leakage	Elastic	Inelastic	N,xN	Total
U238	-481.5	-67.7	108.8	1.8	34.9	-1.5	-405.2
Pu239	-341.9	306.0	17.7	0.5	15.7	-0.3	-2.4
Pu240	-84.5	-72.5	4.5	0.2	4.0	-0.1	-148.4
Am241	-18.4	-17.3	0.6	0.0	0.7	0.0	-34.4
Fe56	-43.6	0.0	9.4	-4.3	-16.1	0.0	-54.5
Cr52	-5.7	0.0	-1.7	-0.3	-4.0	0.0	-11.7
O	6.6	0.0	104.8	21.7	1.3	0.0	134.3
C	-2.0	0.0	267.7	-96.3	-2.5	0.0	166.9
Other	-14.0	4.3	-0.3	2.3	-3.9	0.0	-11.4
Total	-985.0	152.8	511.5	-74.4	30.1	-1.9	-366.8

Table 10. Exact Perturbation Components [pcm] for $\Delta\rho_{\text{graphite_transition}} = \rho_{\text{homogeneous_pit}} - \rho_{\text{heterogeneous_pit}}$

Isotope	Capture	Fission	Leakage	Elastic	Inelastic	N,xN	Total
U238	-632.9	-75.4	97.7	2.2	38.0	-1.7	-572.1
Pu239	-450.1	481.8	16.5	0.6	15.8	-0.3	64.2
Pu240	-109.0	-75.3	4.2	0.2	4.0	-0.1	-176.0
Am241	-23.5	-18.0	0.5	0.0	0.7	0.0	-40.3
Fe56	-51.2	0.0	9.1	-4.1	-15.1	0.0	-61.2
Cr52	-6.5	0.0	-1.9	-0.2	-3.7	0.0	-12.3
Ni58	-2.8	0.0	-1.8	2.2	-1.0	0.0	-3.3
O	6.9	0.0	91.6	24.9	1.3	0.0	124.7
C	-2.4	0.0	255.8	-106.9	-2.9	0.0	143.6
Other	-13.4	7.5	3.0	-0.1	-2.5	0.0	-5.6
Total	-1284.9	320.6	474.7	-81.2	34.6	-2.1	-538.3

Table 11. Exact Perturbation Components by Energy Group for the Reference Configuration [pcm].

Gr.	Energy [eV]	$\Delta\rho_{\text{reference}} = \rho_{\text{homogeneous_pit}} - \rho_{\text{heterogeneous_pit}}$							
		U238 Capture	U238 Leakage	Pu239 Capture	Pu239 Fission	Pu240 Capture	O Leakage	C Leakage	C Elastic
1	1.9640E+7	0.0	0.8	0.0	-21.0	0.0	0.5	0.7	-1.5
2	6.0653E+6	0.8	8.9	0.5	-171.1	0.3	5.1	23.7	-12.0
3	2.2313E+6	0.8	7.6	1.0	-93.8	0.4	6.4	20.3	-10.5
4	1.3534E+6	7.0	15.0	2.5	-124.9	0.6	22.4	56.7	-19.7
5	4.9787E+5	4.2	17.5	2.1	-38.1	0.4	25.7	56.7	-12.6
6	1.8316E+5	-1.4	20.0	-0.4	4.0	-0.1	16.4	56.9	-0.8
7	6.7379E+4	-15.0	15.1	-2.6	24.4	-0.9	10.3	34.0	1.8
8	2.4788E+4	-36.1	11.9	-8.1	37.3	-1.9	7.5	21.1	-14.4
9	9.1188E+3	-147.1	6.3	-45.5	121.0	-7.6	3.4	8.2	-14.2
10	2.0347E+3	-202.7	1.1	-122.7	251.0	-20.6	0.7	1.9	-19.0
11	4.5400E+2	-141.5	-1.8	-196.0	337.3	-51.0	-1.4	-2.1	-8.6
12	2.2603E+1	-18.4	-0.4	-14.6	39.2	-1.5	-0.3	-0.4	0.4
13	4.0000E+0	0.0	-0.1	-1.6	12.3	-11.9	-0.1	-0.1	1.0
14	5.4000E-1	0.0	0.0	-1.8	3.0	-0.3	0.0	0.0	0.0
15	1.0000E-1	0.0	0.0	0.0	0.1	0.0	0.0	0.0	0.0
	Total	-549.4	102.0	-387.0	380.6	-94.2	96.6	277.7	-110.0

Sensitivity Analysis

Sensitivity coefficients have also been calculated as additional parameter for comparing core configurations. The coefficients were obtained using to the following equation:

$$S_j = \partial(\Delta\rho) \frac{\sigma_j}{\partial\sigma_j} = \left\{ \frac{1}{I_f^p} \langle \Phi_p^*, \sigma_{j,p} \Phi_p \rangle - \frac{1}{I_f} \langle \Phi^*, \sigma_j \Phi \rangle \right\}$$

where,

Φ_p^* , Φ_p : adjoint and direct fluxes of the perturbed configuration;

Φ^* , Φ : adjoint and direct fluxes of the reference configuration;

$I_f = \langle \Phi^*, F\Phi \rangle$ and F the fission production operator of the Boltzmann equation $A\Phi = (1/K_{eff}) F\Phi$.

The sensitivity coefficient results are summarized in Tables 12 and 13 by isotope and Tables 14 and 15 by neutron energy group, for the differences between the reference configuration and the configurations containing void and graphite transition zones. For the comparison to the void transition core, the most important sensitivity coefficients are those for (1) U-238 capture, fission, inelastic and v, (2) Pu-239 capture and v, (3) Fe-56, C and O elastic, and (4) Pu-240 capture, fission and v. When the reference and graphite transition zone configurations are compared, the primary sensitivity coefficients arise from (1) U-238 capture, fission, inelastic and v, (2) Pu-239 capture, fission and v, (3) Fe-56, and C elastic, and (4) Pu-240 capture and v. Similar trend in magnitudes of the sensitivity coefficients by energy group, are observed in Tables 14 and 15.

Table 12. Sensitivity Coefficients by Isotopes [pcm] for $\Delta\rho = \rho_{\text{void_transition}} - \rho_{\text{reference}}$ (Heterogeneous).

Isotope	Capture	Fission	v	Elastic	Inelastic	N,XN	Total
U235	9.7	-13.7	-31.2	0.1	-0.5	0.0	-4.4
U238	495.6	110.8	182.1	42.1	-109.1	0.9	540.3
Np237	1.6	0.3	0.5	0.0	0.0	0.0	1.9
Pu238	0.9	0.7	0.8	0.0	0.0	0.0	1.6
Pu239	454.7	16.4	-259.9	5.8	-11.3	0.1	465.7
Pu240	105.4	60.6	84.9	1.5	-3.4	0.0	164.1
Pu241	2.8	-9.8	-19.3	0.1	-0.1	0.0	-7.1
Pu242	3.1	1.6	2.4	0.0	-0.1	0.0	4.7
Am241	45.1	9.4	12.7	0.1	-0.6	0.0	54.0
Fe56	-11.5	0.0	0.0	108.9	-37.9	0.1	59.6
Cr52	-3.0	0.0	0.0	58.6	-8.7	0.0	46.9
Ni58	-15.1	0.0	0.0	20.9	-3.3	0.0	2.5
Si	-0.2	0.0	0.0	4.0	-0.2	0.0	3.6
C	6.9	0.0	0.0	-94.4	9.8	0.0	-77.7
O	-4.4	0.0	0.0	-103.7	-1.4	0.0	-109.5
Total	1091.5	176.4	-27.1	44.1	-166.9	1.2	1146.3

Table 13. Sensitivity Coefficients by Isotopes [pcm] for $\Delta\rho = \rho_{\text{graphite_transition}} - \rho_{\text{reference}}$ (Heterogeneous).

Isotope	Capture	Fission	ν	Elastic	Inelastic	N,XN	Total
U235	-9.9	9.4	26.3	-0.1	0.6	0.0	0.0
U238	-396.8	-132.4	-211.6	-28.7	132.8	-0.7	-425.9
Np237	-1.7	-0.4	-0.5	0.0	0.0	0.0	-1.9
Pu238	-1.0	-0.8	-0.9	0.0	0.0	0.0	-1.7
Pu239	-443.3	-116.6	179.2	-4.2	12.9	-0.1	-551.1
Pu240	-109.5	-62.4	-85.9	-1.2	3.9	0.0	-169.3
Pu241	-2.8	7.5	16.9	-0.1	0.2	0.0	4.8
Pu242	-3.0	-1.7	-2.4	0.0	0.1	0.0	-4.6
Am241	-43.9	-10.2	-13.6	-0.1	0.6	0.0	-53.6
Fe56	20.1	0.0	0.0	-106.0	43.1	-0.1	-42.9
Cr52	5.7	0.0	0.0	-48.7	9.9	0.0	-33.1
Ni58	16.2	0.0	0.0	-27.5	3.8	0.0	-7.6
Si	0.2	0.0	0.0	-3.3	0.2	0.0	-2.8
C	-5.9	0.0	0.0	249.6	-8.3	0.0	235.5
O	4.6	0.0	0.0	63.5	1.4	0.0	69.6
Total	-970.9	-307.6	-92.4	93.4	201.2	-0.9	-984.8

Table 14. Sensitivity Coefficients by Group [pcm] for $\Delta\rho = \rho_{\text{void_transition}} - \rho_{\text{reference}}$ (Heterogeneous).

Gr.	Energy [eV]	Capture	Fission	ν	Elastic	Inelastic	N,XN	Total
1	1.9640E+7	2.1	19.8	31.6	3.6	-3.7	1.2	22.9
2	6.0653E+6	-10.2	162.3	249.7	92.9	-57.2	0.0	187.8
3	2.2313E+6	-4.1	55.8	92.0	89.5	-60.6	0.0	80.6
4	1.3534E+6	-54.8	340.2	476.6	201.7	-28.1	0.0	459.0
5	4.9787E+5	-79.3	344.4	472.6	144.2	-4.7	0.0	404.6
6	1.8316E+5	-97.3	330.7	440.7	94.7	-10.6	0.0	317.5
7	6.7379E+4	-30.7	131.8	154.4	-38.3	-1.8	0.0	61.0
8	2.4788E+4	77.2	-9.7	-43.0	-106.8	-0.1	0.0	-39.5
9	9.1188E+3	370.4	-291.5	-451.4	-200.7	-0.1	0.0	-121.9
10	2.0347E+3	513.3	-493.6	-771.6	-159.0	0.0	0.0	-139.3
11	4.5400E+2	403.5	-410.5	-673.3	-72.5	0.0	0.0	-79.6
12	2.2603E+1	2.7	-3.9	-6.0	-4.7	0.0	0.0	-5.9
13	4.0000E+0	-0.8	0.3	0.4	-0.2	0.0	0.0	-0.8
14	5.4000E-1	-0.1	0.1	0.2	-0.1	0.0	0.0	-0.1
15	1.0000E-1	0.0	0.0	0.0	0.0	0.0	0.0	0.0
Total		1091.5	176.4	-27.1	44.1	-166.9	1.2	1146.3

Table 15. Sensitivity Coefficients [pcm] for $\Delta\rho = \rho_{\text{graphite_transition}} - \rho_{\text{reference}}$ (Heterogeneous).

Gr.	Energy [eV]	Capture	Fission	ν	Elastic	Inelastic	N,XN	Total
1	1.9640E+7	-1.1	-20.8	-32.3	-2.5	4.6	-0.9	-20.7
2	6.0653E+6	10.5	-173.5	-264.6	-98.4	79.2	0.0	-182.1
3	2.2313E+6	5.0	-91.4	-139.6	-77.8	70.5	0.0	-93.7
4	1.3534E+6	42.5	-285.5	-392.5	-123.2	35.7	0.0	-330.4
5	4.9787E+5	65.3	-303.2	-407.7	-79.5	5.0	0.0	-312.5
6	1.8316E+5	91.1	-319.5	-420.1	-55.0	6.6	0.0	-276.7
7	6.7379E+4	78.6	-206.0	-255.7	21.8	0.1	0.0	-105.5
8	2.4788E+4	17.5	-92.9	-101.9	67.7	-0.6	0.0	-8.2
9	9.1188E+3	-200.2	113.9	198.2	181.3	0.0	0.0	94.9
10	2.0347E+3	-451.8	414.5	655.4	177.7	0.0	0.0	140.4
11	4.5400E+2	-608.8	633.3	1032.1	76.0	0.0	0.0	100.5
12	2.2603E+1	-19.9	23.2	36.1	4.2	0.0	0.0	7.5
13	4.0000E+0	0.4	0.3	0.4	0.8	0.0	0.0	1.5
14	5.4000E-1	0.1	-0.1	-0.2	0.1	0.0	0.0	0.1
15	1.0000E-1	0.0	0.0	0.0	0.0	0.0	0.0	0.0
Total		-970.9	-307.6	-92.4	93.4	201.2	-0.9	-984.8

VI. Spectral Index Variations

The spectral indices $\frac{\langle \sigma_{\text{fiss,U8}} \Phi \rangle}{\langle \sigma_{\text{fiss,U5}} \Phi \rangle}$ and $\frac{\langle \sigma_{\text{fiss,Pu9}} \Phi \rangle}{\langle \sigma_{\text{fiss,U5}} \Phi \rangle}$ have been calculated at the core center. The calculations were done using the BISTRO code in RZ geometry and with the S_4P_1 approximation. The fuel cross-sections were processed with the heterogeneous cell calculation.

Results for the reference and void and graphite transition zone configurations are presented in Table 16. Besides the spectral indices, the relative values of the indices to that of the reference configuration are also provided in the table (in brackets).

Table 16. Spectral Indices for ENIGMA Configurations.

Spectral Indices	Reference	Void Transition Zone	Graphite Transition Zone
$\langle \sigma_{\text{f,U8}} \Phi \rangle / \langle \sigma_{\text{f,U5}} \Phi \rangle$	0.029	0.037 (26%)	0.023 (-20%)
$\langle \sigma_{\text{f,Pu9}} \Phi \rangle / \langle \sigma_{\text{f,U5}} \Phi \rangle$	0.908	0.993 (9%)	0.847 (-7%)

The results indicate that large variations in the spectral indices can be achieved by the use of the void and graphite transitional zones. The change is over 60% between the void and graphite transition zone cases for $\langle \sigma_{\text{f,U8}} \Phi \rangle / \langle \sigma_{\text{f,U5}} \Phi \rangle$ and over 16% for $\langle \sigma_{\text{f,Pu9}} \Phi \rangle / \langle \sigma_{\text{f,U5}} \Phi \rangle$.

As in the case of the reactivity variation study, the perturbation components of spectral index variations have been calculated and are provided in Tables 17 to 21. In these calculations only the effects due to flux variations (so-called indirect effects) have been taken into account. Those due to detector cross-section variations (direct effects) have not been considered.

It is observed that the presence or substitution of graphite (C), through its elastic reaction, is responsible for most of the spectral index variation. It however gives contributions with opposite signs for the two transition zone cases; this is true for the two types of spectral indices considered. The breakdown by energy group shows that those contributions are mainly from the energy range where the neutron spectrum is of most importance. In general this study stresses the role that graphite cross-sections, as previously observed in the reactivity section, play for a gas-cooled fast system, and how important it will be to have a rather good accuracy on their values.

Table 17. Exact Perturbation Components for $\left. \frac{\langle \sigma_{U8} \Phi \rangle}{\langle \sigma_{U5} \Phi \rangle} \right|_{(\text{Void Transition - Ref.})/\text{Ref.}}$ (Heterogeneous).

Isotope	Capture	Fission	Leakage	Elastic	Inelastic	N,xN	Total
U238	-0.0017	-0.0002	-0.0002	0.0001	0.0016	0.0000	-0.0005
Pu239	-0.0002	-0.0024	-0.0001	0.0000	0.0003	0.0000	-0.0024
Fe56	0.0003	0.0000	0.0016	-0.0021	-0.0121	0.0000	-0.0122
Cr52	0.0001	0.0000	0.0003	-0.0008	-0.0026	0.0000	-0.0030
Ni58	-0.0002	0.0000	0.0002	-0.0003	-0.0010	0.0000	-0.0013
C	0.0009	0.0000	-0.0135	0.2525	0.0054	0.0000	0.2453
Others	0.0001	-0.0003	0.0007	-0.0005	-0.0026	0.0000	-0.0028
Total	-0.0007	-0.0029	-0.0110	0.2489	-0.0110	0.0000	0.2231

Table 18. Exact Perturbation Components for $\left. \frac{\langle \sigma_{Pu9} \Phi \rangle}{\langle \sigma_{U5} \Phi \rangle} \right|_{(\text{Void Transition - Ref.})/\text{Ref.}}$ (Heterogeneous).

Isotope	Capture	Fission	Leakage	Elastic	Inelastic	N,xN	Total
U238	-0.0006	-0.0001	-0.0001	0.0000	0.0002	0.0000	-0.0006
Pu239	-0.0001	-0.0005	0.0000	0.0000	0.0000	0.0000	-0.0006
Fe56	0.0001	0.0000	0.0004	-0.0005	-0.0006	0.0000	-0.0006
Cr52	0.0000	0.0000	0.0001	-0.0002	-0.0001	0.0000	-0.0002
O	0.0000	0.0000	-0.0001	0.0006	0.0000	0.0000	0.0005
C	0.0001	0.0000	-0.0069	0.0896	0.0001	0.0000	0.0828
Others	0.0001	0.0000	0.0001	-0.0004	-0.0002	0.0000	-0.0003
Total	-0.0004	-0.0006	-0.0065	0.0891	-0.0006	0.0000	0.0810

Table 19. Exact Perturbation Components for $\left. \frac{\langle \sigma_{U8} \Phi \rangle}{\langle \sigma_{U5} \Phi \rangle} \right|_{(\text{Graphite Transition - Ref.})/\text{Ref.}}$ (Heterogeneous).

Isotope	Capture	Fission	Leakage	Elastic	Inelastic	N,xN	Total
U238	0.0044	0.0002	-0.0008	-0.0001	-0.0014	0.0000	0.0022
Pu239	0.0012	0.0039	-0.0002	0.0000	-0.0003	0.0000	0.0046
Fe56	-0.0006	0.0000	0.0007	0.0026	0.0121	0.0000	0.0147
Cr52	-0.0001	0.0000	-0.0001	0.0007	0.0026	0.0000	0.0031
Ni58	0.0002	0.0000	0.0004	0.0008	0.0010	0.0000	0.0023
O	0.0000	0.0000	-0.0005	-0.0005	0.0000	0.0000	-0.0009
C	-0.0008	0.0000	-0.0143	-0.2773	-0.0051	0.0000	-0.2976
Others	-0.0006	0.0002	0.0010	0.0016	0.0025	0.0000	0.0049
Total	0.0037	0.0043	-0.0138	-0.2722	0.0114	0.0000	-0.2667

Table 20. Exact Perturbation Components for $\left. \frac{\langle \sigma_{Pu9} \Phi \rangle}{\langle \sigma_{U5} \Phi \rangle} \right|_{(\text{Graphite Transition - Ref.})/\text{Ref.}}$ (Heterogeneous).

Isotope	Capture	Fission	Leakage	Elastic	Inelastic	N,xN	Total
U238	0.0014	0.0000	-0.0003	0.0000	-0.0001	0.0000	0.0011
Pu239	0.0004	0.0009	-0.0001	0.0000	0.0000	0.0000	0.0012
Fe54	0.0000	0.0000	0.0000	0.0001	0.0000	0.0000	0.0002
Fe56	-0.0002	0.0000	0.0004	0.0007	0.0006	0.0000	0.0015
Cr52	0.0000	0.0000	0.0000	0.0001	0.0001	0.0000	0.0002
Cr53	-0.0001	0.0000	0.0001	0.0001	0.0000	0.0000	0.0002
Ni58	0.0000	0.0000	0.0001	0.0004	0.0000	0.0000	0.0005
C	0.0000	0.0000	-0.0057	-0.0929	-0.0001	0.0000	-0.0987
Others	-0.0002	0.0000	0.0003	0.0003	0.0002	0.0000	0.0003
Total	0.0013	0.0009	-0.0052	-0.0912	0.0007	0.0000	-0.0935

Table 21. Exact Perturbation Components by Energy Group.

Grp	Energy [eV]	Heterogeneous Pit		Homogeneous Pit	
		$\frac{\langle \sigma_{U8} \Phi \rangle}{\langle \sigma_{U5} \Phi \rangle}_{(\text{Void Transition - Ref.})/\text{Ref.}}$	$\frac{\langle \sigma_{Pu9} \Phi \rangle}{\langle \sigma_{U5} \Phi \rangle}_{(\text{Void Transition - Ref.})/\text{Ref.}}$	$\frac{\langle \sigma_{U8} \Phi \rangle}{\langle \sigma_{U5} \Phi \rangle}_{(\text{Graphite Transition - Ref.})/\text{Ref.}}$	$\frac{\langle \sigma_{Pu9} \Phi \rangle}{\langle \sigma_{U5} \Phi \rangle}_{(\text{Graphite Transition - Ref.})/\text{Ref.}}$
1	1.9640E+7	0.0018	0.0000	-0.0017	0.0000
2	6.0653E+6	0.0407	0.0003	-0.0391	-0.0003
3	2.2313E+6	0.0739	0.0020	-0.0768	-0.0021
4	1.3534E+6	0.0286	0.0135	-0.0241	-0.0109
5	4.9787E+5	0.0228	0.0197	-0.0189	-0.0164
6	1.8316E+5	0.0270	0.0224	-0.0239	-0.0199
7	6.7379E+4	0.0228	0.0167	-0.0249	-0.0181
8	2.4788E+4	0.0194	0.0099	-0.0270	-0.0137
9	9.1188E+3	0.0112	0.0044	-0.0233	-0.0091
10	2.0347E+3	0.0046	0.0013	-0.0156	-0.0043
11	4.5400E+2	-0.0003	-0.0007	-0.0020	0.0020
12	2.2603E+1	0.0000	0.0000	0.0000	0.0000
13	4.0000E+0	0.0000	0.0000	0.0000	0.0000
14	5.4000E-1	0.0000	0.0000	0.0000	0.0000
15	1.0000E-1	0.0000	0.0000	0.0000	0.0000
Total		0.2525	0.0896	-0.2773	-0.0929

VII. Conclusions

In this study on GFR physics experiments, the impacts of introducing a transition zone in the central region of the ENIGMA reference configuration on the flux spectrum, core reactivity, and spectral indices have been evaluated. The transition zone would be used in the CEA-Cadarache MASURCA core for the purpose of effecting spectral changes. This would be quite useful if such zones could be utilized for studying physics effects that could not be otherwise obtained in the initial phases of the ENIGMA test due to the potential lack of exact GFR design materials. To obtain the particular zones considered in this work, the central reference subassemblies for the initial phases of the ENIGMA experiment have been modified by replacing all the void rodlets in the subassembly with graphite rodlets (graphite transition zone) or by replacing all the graphite rodlets in the assembly with void rodlets (void transition zone). Both rodlets are used in the reference core subassemblies to simulate carbide fuel, matrix and structural elements and neutron streaming of GFR subassembly designs.

The calculations for the study were performed using the BISTRO and TGV/VARIANT codes, in order to compare trends in solution approaches (RZ versus XYZ models). The impact of the heterogeneous versus homogeneous cross-section generation models was also evaluated. The BISTRO solutions were additionally used in perturbation and sensitivity studies that were performed to understand differences between core configurations and between the cross-section generation approximations.

The results show that significant variations in the neutron flux could be effected by the use of transition zones. The use of a graphite transition zone results in a significantly softer spectrum, while the use of the void transition zone produces a significantly harder spectrum compared to the reference case.

A detailed evaluation of the reactivity variation due to replacement of the central assembly was performed using perturbation theory to investigate components (contributions) of the differences in reactivities for the core configurations. It was observed that the modification to the central zone of the reference configuration results in a slightly higher multiplication factor whether the graphite or void transition zone is used. This was found to be due to variations in the graphite elastic and transport (leakage) components. These components were observed to have different signs for the graphite and void transition zone cases; the leakage component is negative and the elastic component is positive for the void transition zone configuration relative to the reference configuration. However, in both cases, the component with the positive sign dominates. The small magnitude of the reactivity differences between the void and graphite transition configurations and

the reference configuration (<100 pcm) suggests that modifications can be made to the central subassemblies without the need for significant modifications to the control rod designs.

The processing of the cross-section using a homogeneous assembly model in the ECCO code results in significant difference (~400-500 pcm) relative to the case using a heterogeneous assembly treatment. This effect was found higher than that observed in previous calculations for sodium-cooled MASURCA cells (e.g., in the MUSE experiments). Most of the difference between the two models was attributed to the misprediction of the resonance self-shielding of the heavy nuclides; mainly U-238 capture and Pu-239 capture and fission. Some secondary effects come from the elastic reaction in graphite.

The evaluation of variations in the spectral indices $\frac{\langle \sigma_{\text{fiss,U8}} \Phi \rangle}{\langle \sigma_{\text{fiss,U5}} \Phi \rangle}$ and $\frac{\langle \sigma_{\text{fiss,Pu9}} \Phi \rangle}{\langle \sigma_{\text{fiss,U5}} \Phi \rangle}$ at the core center

also indicated significant differences between the reference configuration and the configurations with the void and graphite transition zones. The use of the transition zones could result in the change of the first spectral index by 50% and the second by >16%. Perturbation theory evaluations indicated that these differences are predominantly due to changes in the graphite elastic reaction.

Overall, the results show that the modification of the reference core to a configuration with void or graphite transition zone could be useful as a means of effecting changes in the neutron spectra, with limited impacts on the core reactivity. Moreover, particular emphasis should be put in having good quality graphite cross-sections in view of their dominant role in all the results obtained in this study.

References

1. J. Tommasi, "The ENIGMA Program in MASURCA: Motivation and Presentation," N. T. DER/SPRC/LEPh 04-207, Commissariat à l'Energie Atomique, France (2005).
2. G. Palmiotti, R. F. Burstall, E. Kiefhaber, W. Gebhardt, J. M. Rieunier, "New Methods Developments and Rationalization of Tools for LMFBR Design in the Frame of the European Collaboration," FR'91 International Conference on Fast Reactors and Related Fuel Cycles, Kyoto, Japan, October 28 – November 1, 1991.
3. G. Rimpault, "Algorithmic Features of the ECCO Cell Code for treating Heterogeneous Fast Reactor Assemblies," International Topical Meeting on Reactor Physics and Computation, Portland – Oregon, May 1-5, 1995.
4. E. Fort, W. Assal, G. Rimpault, J. L. Rowlands, P. Smith, R. Soule, "Realization and Performance of the Adjusted Nuclear Data Library ERALIB1 for Calculating Fast Reactor Neutronics," PHYSOR96, Mito, Japan, 1996.
5. G. Palmiotti, J. M. Rieunier, C. Gho, M. Salvatores, "BISTRO Optimized Two Dimensional Sn Transport Code", *Nucl. Sci. Eng.*, **104**, 26 (1990).
6. G. Palmiotti, C. B. Carrico, E. E. Lewis, "Variational Nodal Transport Methods with Anisotropic Scattering," *Nucl. Sci. Eng.*, **115**, p.233 (1993).